

Classification of pulsars with Dirichlet process Gaussian mixture model

Fahrettin Ay¹, Gökhan İnce¹, Mustafa E. Kamaşak¹, K. Yavuz Ekşi²

¹ Istanbul Technical University, Faculty of Computer and Informatics, Computer Engineering Department, 34469, İstanbul, Turkey

² Istanbul Technical University, Faculty of Science and Letters, Physics Engineering Department, 34469, İstanbul, Turkey

ABSTRACT

Young isolated neutron stars (INS) most commonly manifest themselves as rotationally powered pulsars (RPPs) which involve conventional radio pulsars as well as gamma-ray pulsars (GRPs) and rotating radio transients (RRATs). Some other young INS families manifest themselves as anomalous X-ray pulsars (AXPs) and soft gamma-ray repeaters (SGRs) which are commonly accepted as magnetars, i.e. magnetically powered neutron stars with decaying super-strong fields. Yet some other young INS are identified as central compact objects (CCOs) and X-ray dim isolated neutron stars (XDINs) which are cooling objects powered by their thermal energy. Older pulsars, as a result of a previous long episode of accretion from a companion, manifest themselves as millisecond pulsars and more commonly appear in binary systems. We use Dirichlet process Gaussian mixture model (DPGMM), an unsupervised machine learning algorithm, for analyzing the distribution of these pulsar families in period P and period derivative \dot{P} parameter space. We compare the average values of the characteristic age, magnetic dipole field strength, surface temperature and proper motion of all discovered components. We verify that DPGMM is robust and provides hints for inferring relations between different classes of pulsars. We discuss the implications of our findings for the magnetothermal spin evolution models and fallback discs.

Key words: methods: data analysis – methods: statistical – stars: neutron – pulsars: general

1 INTRODUCTION

Rotationally powered pulsars (RPPs), the most common manifestation of neutron stars, were discovered first as radio pulsars (Hewish et al. 1968). More than ~ 2600 RPPs discovered to date are understood to be strongly magnetized ($B \sim 10^{12}$ G), rapidly rotating (with spin periods $P \sim 0.1$ s) neutron stars spinning down by torques due to magnetic dipole radiation and particle emission. These objects emit most of the energy, tapped from their rotational kinetic energy, in X- and gamma-ray bands. The total radiative luminosity of RPPs is thus below their spin-down power $L_{\text{sd}} \equiv -I\Omega\dot{\Omega}$ where I is the moment of inertia of the compact object, $\Omega = 2\pi/P$ is the spin angular frequency and $\dot{\Omega}$ is its time derivative (see Manchester 2017, for a review). The bulk of the RPP population are the classical radio pulsars with periods $P = 0.2 - 2$ s, period derivatives $\dot{P} = 10^{-16} - 10^{-13}$ s s⁻¹, magnetic fields $B \sim 10^{10} - 10^{13}$ G and characteristic ages $\tau_c \equiv P/2\dot{P} \sim 10^3 - 10^7$ years. Some of the RPPs are associated with supernova remnants (SNRs). Young RPPs are usually isolated objects in the sense that they have no binary companion. The pulsations are at-

tributed to the beaming of the emitted radiation and the “lighthouse” effect produced by the spin of the object. Thus, apart from distant and dim objects, there could be many RPPs whose beam does not sweep our line of sight.

A population among the RPPs are the millisecond pulsars (MSP; Backer et al. 1982) which are old but “recycled” pulsars (Alpar et al. 1982); these objects are understood to descend from low-mass X-ray binaries (LMXBs; see Bhattacharya & van den Heuvel 1991; Tauris & van den Heuvel 2006, for reviews) where the neutron star spins-up by accreting matter from a companion via a disc. The accreted matter transfers angular momentum to the neutron star thereby spinning it up to millisecond periods and the magnetic field of the neutron star is reduced to values $B < 10^9$ G in the process.

More than 200 γ -ray pulsars (GRPs) discovered by the Large Area Telescope onboard Fermi (Fermi-LAT; Atwood et al. 2009) constitute a subclass of RPPs (Abdo et al. 2010, 2013). All known GRPs have $L_{\text{sd}} > 10^{33}$ erg s⁻¹. About half of the GRPs detected by Fermi are radio-quiet. This possibly indicates that the “radio beam” which is narrower than the “gamma beam” does not pass from our line of sight.

Approximately half of the discovered GRPs are MSP which was unexpected before the discovery (Abdo et al. 2009).

Another recently discovered family of RPPs is the rotating radio transients (RRATs) identified in the Parkes multi-beam survey (McLaughlin et al. 2006). Unlike ordinary pulsars detected by searches in the frequency domain, RRATs show sporadic emission detected through their bright single pulses. These objects show bursts of duration 2–30 ms with an interval in the range 4 min–3 hr. Their spin periods are in the range 0.4–7 s. The period derivatives are measured in 3 sources implying magnetic fields $B \sim 10^{12} - 10^{14}$ G and characteristic ages $\tau_c \sim 0.1 - 3$ Myr.

In the last two decades many young isolated neutron star (INS) families (see Popov 2008; Kaspi 2010; Harding 2013; Safi-Harb 2017, for reviews) other than radio pulsars are identified. These objects are usually radio-quiet and have X-ray luminosities exceeding the spin-down power of the compact object. This indicates the availability of energy budgets other than rotational kinetic energy and the possibility of evolutionary paths other than those leading to RPPs.

Of these groups of objects soft gamma ray repeaters (SGRs) and anomalous X-ray pulsars (AXPs) are commonly assumed to be magnetars (see Woods & Thompson (2006); Mereghetti (2008); Rea (2014); Turolla et al. (2015); Mereghetti et al. (2015); Kaspi & Beloborodov (2017); Gourgioliatos & Esposito (2018) for reviews) i.e. INSs with large dipole magnetic fields $B \sim 10^{14} - 10^{15}$ G as inferred from their rapid spin down $\dot{P} \sim 10^{-13} - 10^{-11}$ s s⁻¹ (Kouveliotou et al. 1998) and slow periods clustered between $P = 2 - 12$ seconds. According to the magnetar model (Duncan & Thompson 1992; Thompson & Duncan 1996) the persistent X-ray emission of these objects with X-ray luminosity of $L_X \sim 10^{35} - 10^{36}$ erg s⁻¹ is powered by the decay of this strong magnetic field (Paczynski 1992; Thompson & Duncan 1995) in excess of the quantum critical limit $B_{QED} = 4.4 \times 10^{13}$ G. These objects occasionally show super-Eddington outbursts and, very rarely, giant bursts which are addressed in the magnetar model with the breaking of the neutron star crust due to magnetic stresses and reconfiguration of their fields, respectively. The magnetars are young objects as implied by their characteristic ages $\tau_c \sim 10^4$ years and about half of them being associated with SNRs.

X-ray dim isolated neutron stars (XDINs), or sometimes called “magnificent seven”, are the 7 nearby neutron stars identified through their thermal X-ray emission (Özel 2013; Potekhin et al. 2015; Mereghetti 2011) with luminosities of order $L_X \sim 10^{30} - 10^{32}$ erg s⁻¹ (see Haberl 2007; Kaplan 2008; Turolla 2009, for reviews). They have a period range similar to the AXP/SGR family (Hambaryan et al. 2017), but are typically older, with characteristic ages $\tau_c \sim 10^5 - 10^6$ years and kinematic ages of a few 10^6 years (Tetzlaff et al. 2010, 2011, 2012). They have inferred dipole magnetic fields of $B \sim 10^{13}$ G, an order of magnitude lower than magnetars and an order of magnitude higher than conventional pulsars, but their surface magnetic fields as inferred from the narrow absorption features are 7 (Borghese et al. 2015) and 5 (Borghese et al. 2017) times larger in the case of RX J0720.4–3125 and RX J1308.6+2127, respectively.

Yet another young NS family is the central compact objects (CCOs; see De Luca 2017, for a review) in super-

nova remnants (SNRs). These ~ 10 objects show no sign of RPP activity. Their X-ray spectra is dominated by the thermal emission showing some similarities with magnetars yet they are two orders of magnitude less luminous ($\sim 10^{33} - 10^{34}$ erg s⁻¹). The periods measured from 3 CCOs are in the range 0.1–0.4 s and the measured period derivatives imply that the dipole fields of these objects are in the range $B \sim 10^{10} - 10^{11}$ G (Gotthelf & Halpern 2007, 2009; Halpern & Gotthelf 2011), and hence sometimes are called “anti-magnetars” (Halpern & Gotthelf 2010; Gotthelf et al. 2013). Yet there is evidence that these objects have much stronger “hidden” magnetic fields (Viganò & Pons 2012; Viganò et al. 2013; Torres-Forné et al. 2016) as implied by the highly anisotropic emission (Shabaltas & Lai 2011) leading to the observed high pulsed fraction. According to the “field burial scenario” (Muslimov & Page 1995; Young & Channugam 1995; Gepert et al. 1999; Ho 2011; Bernal et al. 2012; Igoshev et al. 2016) this is due to an initial fallback accretion episode the nascent neutron star had suffered soon after the SN explosion. An exception among the CCO family is 1E 161348–5055 in SNR RCW 103 which has an unusually long period of 6.7 hours (de Luca 2008) and has recently shown magnetar-like bursts (Rea et al. 2016).

Recent discoveries are blurring the borders of the classes: (i) The existence of high magnetic field RPPs (Pivovaroff et al. 2000); see Ng & Kaspi (2011) for a review) that have magnetic field strengths comparable and, in some cases, exceeding that of some magnetars and some of which has even shown magnetar-like X-ray bursts (Gavril et al. 2008; Archibald et al. 2016; Gögiş et al. 2016); (ii) radio detection from some magnetars (Camilo et al. 2006, 2007; Levin et al. 2010); (iii) identification of low-magnetic field magnetars (Rea et al. 2010) i.e. INS showing magnetar bursts but with ordinary inferred dipole field strengths (see Turolla & Esposito 2013, for a review). These discoveries indicate that the *dipole* field strength is not the single parameter leading to the different manifestations favouring the early suggestions (Gavril et al. 2002; Ekşioğlu & Alpar 2003; Ertan & Alpar 2003; McLaughlin et al. 2003) that what causes the magnetar activity could be in the higher multipoles (Alpar et al. 2011; Rodríguez Castillo et al. 2016).

In fact there are other observations suggesting that AXP/SGRs have “low” *dipole* fields: (i) They are not detected in the Fermi/LAT observations (Şaşmaz Muş & Gögiş 2010; Abdo et al. 2010) in the GeV range though, according to the outer gap model (Zhang & Cheng 1997), they are expected (Cheng & Zhang 2001) to emit high energy gamma-rays should they have super-strong magnetic dipole fields $\gtrsim 10^{14}$ G (Tong et al. 2011). (ii) their transverse velocities are measured (Helfand et al. 2007; Deller et al. 2012; Tendulkar et al. 2012, 2013) to be 200 ± 100 km s⁻¹, similar to the velocities of RPPs though they are expected to have exceptionally large space velocities, ~ 1000 km s⁻¹, due to getting stronger kicks (Duncan & Thompson 1992; Thompson & Duncan 1993) via the rocket propulsion effect should they have super-strong dipole fields. (iii) They do not commonly show the signature of the expected strong energy injection in the SNRs due to hosting a neutron star with a birth period of milliseconds (Vink & Kuiper 2006; Martin et al. 2014; Borkowski & Reynolds 2017) (but see Torres (2017)) that could produce super-strong fields by dynamo

action (Duncan & Thompson 1992; Thompson & Duncan 1993).

Given the transitivity among the INS families the question naturally arises whether the classification of INS above is robust. Could we expect, for example, that more of the RPPs to show magnetar-like behaviour, or that more magnetars to appear in the radio band? What parameters could be leading to the different manifestations for objects with similar period and period derivatives? The magneto-thermal evolutionary theory (e.g. Viganò & Pons 2012; Viganò et al. 2013) addresses this diversity by the presence of toroidal magnetic fields hidden in the crust as an extra parameter shaping the lives of pulsars. The fallback disc model (Alpar 2001; Chatterjee et al. 2000) invokes the mass and specific angular momentum (Ertan et al. 2007, 2009) of a putative supernova fallback disc as two parameters leading to the diversity.

A well-known unsupervised machine learning algorithm, Gaussian mixture model (GMM; Press et al. 2007), had been used by Lee et al. (2012) to analyze the distribution of pulsars on the $P - \dot{P}$ diagram and identified six Gaussian clusters (two for millisecond—recycled—pulsars and 4 for young pulsars). Igoshev & Popov (2013) showed that GMM is over-sensitive to the data and does not demonstrate robust clustering performance. Besides, there are more advanced variations of GMM such as Dirichlet process Gaussian mixture model (DPGMM). This model has the advantage over GMM that the number of components are determined automatically. In addition its generalization performance is better than GMM, because Bayesian methods are more robust against overfitting (Rasmussen 2000; Heller 2008; Witten et al. 2016). A recent work Del Pozzo et al. (2018) can be given as an example where DPGMM is used to localize binary neutron stars from the gravitational-wave data. However, it is not as famous as GMM especially in astronomy community as far as the authors knowledge. Taking into consideration its advantages, we employed DPGMM in this paper to explore possible hidden components within the INS families and to classify the $P - \dot{P}$ parameter space accordingly.

The organization of our paper is as follows. In § 2 we review DPGMM employed in this work, and test the model on the data set. In § 3 we present our results and finally, in § 4, we discuss the implications of our findings.

2 METHOD

Statistical inference is widely used to model an observed data with a proper probability density function (pdf) and make estimations about the underlying origin of the data. Very often, it is presumed that the data comes from a simple distribution. For example, Gaussian distribution is commonly used for modelling symmetric bell-shaped data. Many real world problems, however, are so complex that there is no single well-defined pdf that can fit to the observations. In addition, it is possible that there are multiple distributions constituting the observed data. In such cases, it is favourable to employ mixture models which provide convenience to model complex data so that they are more applicable to the real world problems than single distribution models.

In this section we start by reviewing Gaussian mixture

model (GMM). The derivation of Bayesian Gaussian mixture model (BGMM) is detailed at the following section. Subsequently, Dirichlet process Gaussian mixture model (DPGMM) that is employed in this study is introduced. We test DPGMM on available pulsar data set and evaluate its outputs at the final section.

2.1 Gauussion mixture model

In finite mixture models, it is assumed that there are fore-known number of distributions that generate the data. Let $\mathbf{X}^T = [\mathbf{x}_1 \mathbf{x}_2 \dots \mathbf{x}_N]$ be the collection of d -dimensional observed data with N number of instances and assume further that there are m distributions that generate \mathbf{X} . Furthermore, assume that the distribution underlying a specific data instance is unknown. Hence, mixture models are called as unsupervised models in machine learning. Therefore, it is useful to define a latent data \mathbf{Z} for distribution assignments; $\mathbf{Z}^T = [z_1 z_2 \dots z_N]$ where $z_j = i$ means that \mathbf{x}_j belongs to i -th distribution, $j \in \{1, 2, \dots, N\}$. and $i \in \{1, 2, \dots, m\}$.

The joint probability of a data point \mathbf{x}_j that is being generated by the i -th component ¹ can be expressed using conditional probability theorem as

$$p(\mathbf{x}_j, z_j = i) = p(\mathbf{x}_j | z_j = i) p(z_j = i) \quad (1)$$

Because \mathbf{x}_j must be populated by one of the m components, we can obtain marginal probability of \mathbf{x}_j from the equation (1) as follows

$$p(\mathbf{x}_j) = \sum_{i=1}^m p(\mathbf{x}_j | z_j = i) p(z_j = i) \quad (2)$$

The probability of \mathbf{x}_j being populated by the i -th component is actually the probability of the i -th component

$$p(z_j = i) \equiv \pi_i \quad (3)$$

where $\sum_{i=1}^m \pi_i = 1$. In addition, if we consider that all components are distributed normally, then the probability of data instance \mathbf{x}_j given that it is being populated by the i -th component becomes a realization from the i -th Gaussian component

$$p(\mathbf{x}_j | z_j = i) \equiv \mathcal{N}(\mathbf{x}_j | \boldsymbol{\mu}_i, \boldsymbol{\Sigma}_i) \quad (4)$$

where the multivariate Gaussian distribution is defined as

$$\mathcal{N}(\mathbf{x}_j | \boldsymbol{\mu}_i, \boldsymbol{\Sigma}_i) = \frac{\exp\left(-\frac{1}{2}(\mathbf{x}_j - \boldsymbol{\mu}_i)^T \boldsymbol{\Sigma}_i^{-1} (\mathbf{x}_j - \boldsymbol{\mu}_i)\right)}{(2\pi)^{d/2} |\boldsymbol{\Sigma}_i|^{1/2}} \quad (5)$$

In this case, the finite mixture model is called as Gaussian mixture model (GMM) where $\boldsymbol{\mu}_i$ is d -length mean vector and $\boldsymbol{\Sigma}_i$ is $d \times d$ covariance matrix of i -th Gaussian component. The pdf of GMM is

$$p(\mathbf{x}_j | \boldsymbol{\theta}) = \sum_{i=1}^m \pi_i \mathcal{N}(\mathbf{x}_j | \boldsymbol{\mu}_i, \boldsymbol{\Sigma}_i) \quad (6)$$

where $\boldsymbol{\theta} = \{\boldsymbol{\pi}, \boldsymbol{\mu}, \boldsymbol{\Sigma}\}$ denotes all model parameters, $\boldsymbol{\pi} = [\pi_1 \pi_2 \dots \pi_m]$ is m -length vector, $\boldsymbol{\mu}^T = [\boldsymbol{\mu}_1 \boldsymbol{\mu}_2 \dots \boldsymbol{\mu}_m]$ is $m \times d$ matrix, and $\boldsymbol{\Sigma}^T = [\boldsymbol{\Sigma}_1 \boldsymbol{\Sigma}_2 \dots \boldsymbol{\Sigma}_m]$ is $m \times d \times d$ tensor.

In this model, the likelihood of the data is assumed to

¹ The term *component* is used hereinafter instead of the term *distribution*

be formed by mixture of Gaussians. Hence, one needs to find optimum parameters that maximize the likelihood of the data in order to “fit” GMM to the observations

$$p(\mathbf{X}|\boldsymbol{\theta}) = \prod_{j=1}^N \sum_{i=1}^m p(\mathbf{x}_j, z_j = i | \boldsymbol{\theta}) \quad (7)$$

$$\hat{\boldsymbol{\theta}} = \arg \max_{\boldsymbol{\theta}} p(\mathbf{X}|\boldsymbol{\theta}) \quad (8)$$

where (7) is the definition of the likelihood of the observed data, and $\hat{\boldsymbol{\theta}}$ is the maximum likelihood of the mixture model parameters. It is not possible to obtain $\hat{\boldsymbol{\theta}}$ analytically due to the complex structure of the likelihood. However, it is possible to obtain an iterative solution. Expectation-Maximization (EM; Dempster et al. 1977) algorithm is a well-known method for approximating $\hat{\boldsymbol{\theta}}$ iteratively. In this method, all parameters $\boldsymbol{\theta} = \{\boldsymbol{\pi}, \boldsymbol{\mu}, \boldsymbol{\Sigma}\}$ are initialized randomly at the first step. Then, two steps — expectation (E-step) and maximization (M-step)— are iterated repeatedly so that the likelihood of data defined in (7) increases at the end of each iteration.

As detailed above, the model parameters are learned by maximizing the likelihood of the data set. However, the observed data is just a subset of the real population whose real distribution cannot be known in the most of the cases. If the observed data is a perfect representation of the real population, then maximum likelihood estimation provides a perfect solution. However, observations usually contain a bias so that its distribution differs from the distribution of the real population. To illustrate, the spin parameters of more than 2000 pulsars are observed so far. It is believed that there are much more neutron stars in our galaxy but most of them are not explorable, at least for now, because of either the technological inabilities or the direction of their emitted beams not pointing to the earth. Therefore, it can be said that we do not know the distribution of the real population of neutron stars and the observed data set contains bias due to the selection effects. Hence, the maximum likelihood estimation may cause “overfitting” which means that the fitted model may suits the observations utterly, but it may not descriptive for the real population as well.

2.2 Bayesian Gaussian mixture model

In Bayesian approach, parameters of the likelihood model are also modeled with a *prior* distribution $p(\boldsymbol{\theta})$. Therefore, the *posterior* of data $p(\boldsymbol{\theta}|\mathbf{X})$ is considered as the complete model. Ignoring the normalizing factor, the posterior is proportional to the product of likelihood of data and the prior of parameters

$$p(\boldsymbol{\theta}|\mathbf{X}) \propto p(\mathbf{X}|\boldsymbol{\theta})p(\boldsymbol{\theta}) \quad (9)$$

If the likelihood model is selected as mixture of Gaussian distributions as in (7), then the posterior model is called as Bayesian Gaussian mixture model (BGMM). In this case, the prior of GMM parameters are defined as below

$$p(\boldsymbol{\theta}) = p(\boldsymbol{\pi}, \boldsymbol{\Sigma}, \boldsymbol{\mu}) = p(\boldsymbol{\pi})p(\boldsymbol{\Sigma}, \boldsymbol{\mu}) \quad (10)$$

If we use the prior given in (10), and extend the likelihood as in (2) for whole data set, then the posterior model can be

defined as

$$p(\boldsymbol{\theta}|\mathbf{X}, \mathbf{Z}) \equiv p(\mathbf{X}|\mathbf{Z}, \boldsymbol{\theta})p(\mathbf{Z}|\boldsymbol{\theta})p(\boldsymbol{\pi})p(\boldsymbol{\Sigma}, \boldsymbol{\mu}) \quad (11)$$

As seen in (11), the posterior model has a complex form with multiple random variables. We know from (4) that $p(\mathbf{X}|\mathbf{Z}, \boldsymbol{\theta})$ is multivariate Gaussian distributed

$$\mathbf{X}|\mathbf{Z}, \boldsymbol{\theta} \sim \mathcal{N}(\boldsymbol{\mu}, \boldsymbol{\Sigma}) \quad (12)$$

In addition, it can be shown that the latent data \mathbf{Z} is multinomial distributed. Let $\mathbf{n} = [n_1 \ n_2 \ \dots \ n_m]$ where n_i denotes the number of data instances belonging to the i -th component so that

$$n_i = \sum_{j=1}^N \delta_i(z_j) \quad \text{and} \quad \delta_i(z_j) = \begin{cases} 1, & \text{if } z_j = i \\ 0, & \text{otherwise} \end{cases}$$

where $\sum_{i=1}^m n_i = N$. Then, the probability of n_1, n_2, \dots, n_m data instances belonging to the 1st, 2nd, ..., m -th components respectively is the form of multinomial distribution

$$p(n_1, \dots, n_m | \boldsymbol{\pi}_1, \dots, \boldsymbol{\pi}_m) = \frac{N!}{n_1! \ n_m!} \prod_{i=1}^m \boldsymbol{\pi}_i^{n_i} \quad (13)$$

$$\boldsymbol{\pi} | \boldsymbol{\pi} \sim \text{Multinomial}(\boldsymbol{\pi}) \quad (14)$$

However, the prior distributions for $\boldsymbol{\theta} = \{\boldsymbol{\pi}, \boldsymbol{\Sigma}, \boldsymbol{\mu}\}$ are unknown. Therefore, they are selected according to “conjugacy” principle due to the computational simplicity. In plain words, for a specific likelihood, if the selected prior is same probability distribution family as the posterior, then it is called as “conjugate” prior (Raiffa & Schlaifer 1961). To illustrate, “Dirichlet distribution” is conjugate prior for multinomial likelihood, and “Normal-Inverse-Wishart” distribution is conjugate prior for multivariate Gaussian likelihood.

Dirichlet distribution is a probability measure over a probability simplex on which any coordinate corresponds to a probability vector whose elements add up to 1. In other words, it is a distribution for probability vectors. Because of its conjugacy property and by taking into consideration that the latent data \mathbf{Z} has a multinomial distribution (13), Dirichlet distribution is a good candidate for selecting prior for $\boldsymbol{\pi}$

$$\boldsymbol{\pi} \sim \text{Dir}(\boldsymbol{\alpha}) \quad (15)$$

$$\boldsymbol{\pi} | \mathbf{Z} \sim \text{Dir}(\boldsymbol{\alpha} + \mathbf{n}) \quad (16)$$

where $\boldsymbol{\alpha} = [\alpha_1 \ \dots \ \alpha_m]$ is concentration parameter consisting of positive real numbers that effects the magnitude of elements in $\boldsymbol{\pi}$ vector. Intuitively, if α_i is relatively higher than the rest of elements in $\boldsymbol{\alpha}$, then the probability of π_i being greater than other elements in $\boldsymbol{\pi}$ is also higher. Reasonably, $\boldsymbol{\alpha}$ is selected as all-is-equal vector such that $\boldsymbol{\alpha} = \alpha_k \mathbf{I}$ where \mathbf{I} is unit vector, when there is no prior knowledge about the probability of components. In this case, the distribution is called as “symmetric” Dirichlet distribution. In addition to this, it can be shown (Bishop 2006) that the posterior of latent data \mathbf{Z} is also Dirichlet with parameter $\boldsymbol{\alpha} + \boldsymbol{\pi}$ as seen in (16). Hence, the posterior model (11) can be simplified by replacing prior (13) and likelihood (15) with the posterior (16).

In the same way, the prior for $\{\boldsymbol{\Sigma}, \boldsymbol{\mu}\}$ is selected as Normal-Inverse-Wishart (NIW) distribution that is conju-

gate prior of multivariate Gaussian likelihood

$$\{\boldsymbol{\mu}, \boldsymbol{\Sigma}\} \sim \mathcal{NIW}(\boldsymbol{m}, \beta, \boldsymbol{\psi}, \vartheta) \quad (17)$$

$$\{\boldsymbol{\mu}, \boldsymbol{\Sigma}\} | \mathbf{X} \sim \mathcal{NIW}(\boldsymbol{m}^*, \beta^*, \boldsymbol{\psi}^*, \vartheta^*) \quad (18)$$

where $\{\boldsymbol{m}, \beta, \boldsymbol{\psi}, \vartheta\}$ are mean, scaling factor, scale matrix and degrees of freedom hyper-parameters of NIW distribution, respectively. It can also be proved (Bishop 2006) that the posterior of $\{\boldsymbol{\Sigma}, \boldsymbol{\mu}\}$ as shown in (18) is also NIW distribution with parameters $\{\boldsymbol{m}^*, \beta^*, \boldsymbol{\psi}^*, \vartheta^*\}$ that can be obtained from previous parameters. Therefore, the posterior model (11) can be simplified once again by replacing prior (12) and likelihood (17) with posterior (18). The final form of the posterior model is

$$p(\boldsymbol{\theta} | \mathbf{X}, \mathbf{Z}) \equiv \text{Dir}(\boldsymbol{\alpha} + \mathbf{n}) \mathcal{NIW}(\boldsymbol{m}^*, \beta^*, \boldsymbol{\psi}^*, \vartheta^*) \quad (19)$$

Because of its Bayesian nature, BGMM is better model in terms of overfitting. However, the major drawback of finite mixture models is that the number of components is not regarded as a part of the problem. One then needs to infer the correct number of components explicitly. The common strategy is to change the number of components according to a certain information criteria. For example, Akaike information criterion (AIC; Akaike 1974) or Bayesian information criterion (BIC; Schwarz 1978) are two statistical methods that are commonly used for determining the number of components for GMM.

2.3 Dirichlet process Gaussian mixture model

Dirichlet process (DP; Ferguson 1973) is infinite-dimensional generalization of Dirichlet distribution parameterized with a *single* concentration parameter α_0 and a base distribution \mathcal{H} . Formally, let Θ be a parameter space and \mathcal{H} be a probability measure on Θ . If G is Dirichlet process distributed

$$G \sim DP(\alpha_0, \mathcal{H}) \quad (20)$$

then for every finite partition $\{A_1 \dots A_K\}$ of Θ

$$(G(A_1), \dots, G(A_K)) \sim \text{Dir}(\alpha_0 \mathcal{H}(A_1) \dots \alpha_0 \mathcal{H}(A_K)) \quad (21)$$

As the partition size (K) can be countably infinite, a drawn from DP can be countably-infinite probability vector as well. In addition, G is *random* probability distribution since $\sum_{i=1}^K G(A_i) = 1$ and \mathcal{H} is random. Specifically, DP is distribution of probability distributions so that a realization G from DP is infinite-length *discrete* probability distribution. Moreover, DP is also conjugate prior for multinomial likelihood. If it is selected as prior for $\boldsymbol{\pi}$

$$\boldsymbol{\pi} \sim DP(\alpha_0, \mathcal{H}) \quad (22)$$

then it can be proved (Gelman et al. 2013) that the posterior for $\boldsymbol{\pi}$ becomes as

$$\boldsymbol{\pi} | \mathbf{Z} \sim DP \left(\alpha_0 + N, \frac{\alpha_0}{\alpha_0 + N} \mathcal{H} + \frac{1}{\alpha_0 + N} \sum_{j=1}^N \delta_{z_j} \right) \quad (23)$$

Hence, we obtain Dirichlet process Gaussian mixture model (DPGMM) by replacing (23) with (16) in posterior model (19). Briefly, DPGMM is a Bayesian non-parametric model so that they are more durable to overfitting problem than GMM, and the number of the mixture components can be

countably infinite depending on the increasing data. The concentration hyper-parameter α_0 take a crucial role in DPGMM. The model has a tendency to discover more components in a given data set together with the increasing α_0 value. Contrarily, the model can be forced to discover less components with a decreasing α_0 value.

In order to fit DPGMM to a data set, the aim is to find parameter sets $\boldsymbol{\theta}$ that maximizes the posterior $p(\boldsymbol{\theta} | \mathbf{X})$. Although the model is simplified according to the conjugacy principle, it is still hard to estimate model parameters. Several approaches introduced to overcome this problem such as Gibbs sampling (Neal 2000) and variational inference (Blei & Jordan 2006). Gibbs sampling is a stochastic model that is computationally expensive. The variational method, however, is faster and it approximates to the exact solution deterministically. For this reason, the variational inference is used in this study to estimate the model parameters.

2.4 Testing the model

In this study, many open source software libraries were used for implementing DPGMM as well as for other scientific computations and analyzes, such as *scikit-learn* (Pedregosa et al. 2011), *scipy* (Jones et al. 01), *numpy* (Oliphant 2006), *pandas* (McKinney et al. 2010). In addition *matplotlib* (Hunter 2007), *seaborn* (Waskom et al. 2017) and *scikit-image* (van der Walt et al. 2014) were used for visualization. Moreover, *spyder*² and *ipython* (Pérez & Granger 2007) programs were used as platforms for implementations and analyzes.

2.4.1 Data Collection

In this study, the distribution of *common* logarithm of pulsar spin parameters is examined; $\mathbf{X} = [\log(\mathbf{P}) \log(\dot{\mathbf{P}})]$. Thus, various neutron star catalogs are combined in order to increase data samples as much as possible. Most of the pulsar data is obtained from Australia Telescope National Facility (ATNF) Pulsar Catalog³ that contains up to 2658 instances with numerous source types. In addition, SGPs and AXPs (30 instances of either confirmed or candidates) are collected from McGill Online Magnetar Catalog⁴ (Olausen & Kaspi 2014). The amount of 40 instances of other thermally emitting neutron stars such as CCOs and XDINs are taken from Viganò et al. (2013)⁵. Additionally, 107 RRATs are taken from RRATOLOG⁶ (McLaughlin et al. 2006; Keane et al. 2010). Finally, 117 GRPs are obtained from *The Second Fermi-LAT catalogue*⁷ (Abdo et al. 2013). The spin parameters of many pulsars are not available in the catalogs. Therefore, we obtained amount of 2165 INSSs with observed spin parameters by combining all these data sources. Moreover, recently discovered (Tan et al. 2018) RPP with an exceptional long period is also included to the data set.

² <https://www.spyder-ide.org/>

³ <http://www.atnf.csiro.au/research/pulsar/psrcat/>

⁴ <http://www.physics.mcgill.ca/~pulsar/magnetar/main.html>

⁵ <http://www.neutronstarcooling.info/>

⁶ <http://astro.phys.wvu.edu/rratalog/>

⁷ <https://heasarc.gsfc.nasa.gov/W3Browse/fermi/fermil2psr.html>

2.4.2 Tuning the hyper-parameter

In fact, DPGMM contains many hyper-parameters. We focus, however, on the concentration parameter α_0 that has the most dramatic effect on the model performance. As mentioned in § 2.3, α_0 is a positive real number and determines how conservative the data is so that the algorithm tends to discover more components for higher values of α_0 . In addition to this, the model needs one more hyper-parameter (N_{max}) in practice. Although DPGMM is an infinite mixture model, it is not practicable to consider infinite number of components. Therefore, the model is restricted with N_{max} corresponding to maximum number of components. For this reason, N_{max} is also considered as hyper-parameter and the optimal α_0 value is searched consequently.

In Figure 1, the average likelihood scores — how well the model is fitted to the data set — and the number of discovered components for models created with different N_{max} and α_0 are illustrated. Although DPGMM is a posterior model, it is fair to compare models according to their likelihood scores because the prior distribution is same for all models. When concentration parameter is set to very low number as $\alpha_0 = 10^{-8}$, models are forced to discover less components. As seen in the figure, all three models with $\alpha_0=10^{-8}$ values have discovered 6 components. It is significant to note that all three models with $\alpha_0=10^{10}$ value have also discovered 6 components despite the models are released to be able to discover more components due to the very large value of α_0 . In addition, 29 of 33 different models have discovered 6 components so that it is reasonable to accept that there are 6 components in the $P - \dot{P}$ parameter space as Lee et al. (2012) have showed using GMM before.

Eventually, N_{max} is selected as 10, because all 11 models with $N_{max} = 10$ have discovered 6 components. In addition, it is observed that estimated component parameters of all models with $N_{max} = 10$ and $\alpha_0 < 10$ have slight differences. Therefore, the selection of α_0 value does not affect the model performance dramatically. Nevertheless, the α_0 is selected as 10^{-5} because all three models with same α_0 value have discovered 6 components.

2.4.3 Application of DPGMM

After determining the hyper-parameters of DPGMM, the model is created with $N_{max} = 10$ and $\alpha_0 = 10^{-5}$ and fitted to $P - \dot{P}$ parameter space of pulsar data set. The estimated component parameters are illustrated in Table 1. The $P - \dot{P}$ diagram with the discovered components and the corresponding regions are illustrated in Figure 2 where the Gaussian components are represented both with the confidence ellipses and Voronoi regions.

Although DPGMM is an unsupervised method, it can also be used for classification purpose. After the model is fitted to the data set, it can predict the label of a novel instance, which component that new instance belongs to, by computing weighted probabilities of that instance with respect to each component separately and selecting the most probable one. In this study, the $P - \dot{P}$ parameter space is classified by using this approach. As a result, the parameter space is partitioned into 6 regions for each component as seen in Figure 2. This approach is actually the estimation of Voronoi cells by using a probabilistic distance metric.

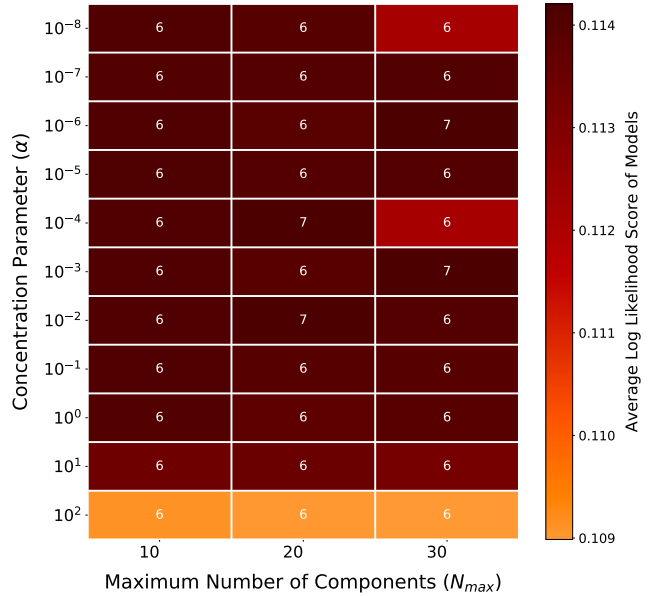


Figure 1. Tuning hyper-parameters of DPGMM. The x-axis and y-axis represent the maximum number of components (N_{max}) and concentration parameter (α_0), respectively. Models are created and tested for each different N_{max} and α_0 values and the number of components discovered by these models is placed in the corresponding cell. The average likelihood score of each model is also illustrated with sequential colors.

Confidence ellipse representation considers only the location (μ) and shape (Σ) of the components together with a confidence interval (σ). On the other hand, the Voronoi region representation considers all component parameters including the component weights π . This suggests that the Voronoi region representation is more descriptive and provides a better illustration of the components than the confidence ellipses; as such it may give clues about the pulsar classification in the $P - \dot{P}$ parameter space. Moreover, it is significant that the confidence ellipses of the components discovered by GMM illustrated in Lee et al. (2012) and DPGMM as seen in Figure 2 look similar. We have seen, though not present in this manuscript, that the Voronoi regions of GMM components are quite different from Voronoi regions of DPGMM components.

In addition, there is a handicap of Voronoi regions representation on Gaussian spaces. Because the distance metric used in this study is non-deterministic so that it depends on the Mahalanobis distance (Mahalanobis 1936; De Maesschalck et al. 2000) which is used to measure distance in terms of standard deviation, there may be more than one region for a single component on Euclidean spaces. To illustrate, it seems that there are two regions colourized with yellow for the 6th component in Figure 3. It is obvious that there should not be a separating line between the 2nd and the 6th component and the lower region of the 6th component should belong to the 2nd component. Therefore, the *dependability* of separating lines are also examined in this study. As mentioned in § 2.4.2, the estimated component parameters for DPGMM slightly change even if hyper-parameters are dramatically changed. On the contrary, the Voronoi regions are sensitive to the model parameters. It is observed when

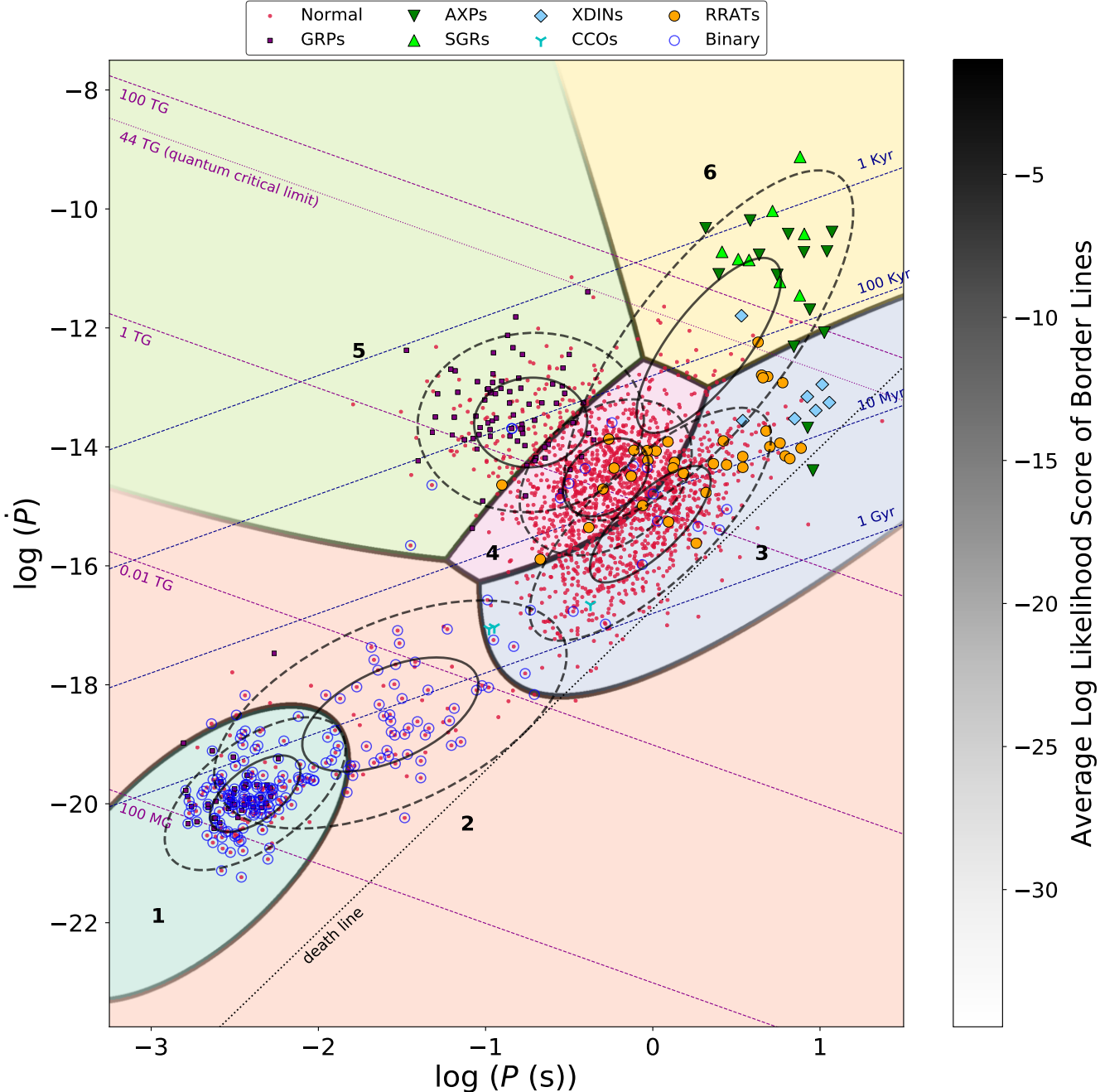


Figure 2. $P - \dot{P}$ diagram with Gaussian components and corresponding Voronoi regions as obtained by DPGMM with $\alpha_0 = 10^{-5}$. Gaussian components are represented by 1σ (solid) and 2σ (dashed) ellipses. Each Voronoi region is colored differently. Component regions are enumerated and their numbers are located inside the corresponding area. The border of regions are represented with thick solid lines of varying shades: The border line is darker where it is more robust, and it is fainter where it is less robust. The robustness is described as the average likelihood of data points that are placed on the border line.

tuning the hyper-parameters of the model that the location of border lines are changed significantly where the average likelihood score of data points over the border line are relatively lower, and they are almost not changed where the same score is relatively higher. Therefore, the dependability of border lines are evaluated according to their likelihood scores. In Figure 2 and Figure 3, the robustness of border lines are also illustrated so that the color of border line is darker where it is more robust, and it is fainter where the

line is less robust. Accordingly, it is obvious that the color of the border line between the 2nd and the 6th components in Figure 3 is very faint that means it is not reliable as expected. In this way, we tried to eliminate the handicap of Voronoi representation in Gaussian spaces.

As seen in Figure 2, the 1st and the 2nd regions contain mostly millisecond pulsars. It is significant that millisecond pulsars are separated into two subclasses as in the case of GMM Lee et al. (2012). In § 4 we discuss the possible ori-

DPGMM Component Parameters				
<i>Id</i>	π	μ	Σ	
1	0.0787	[-2.3782 -19.8306]	[0.0731 0.1019 0.1019 0.4127]	
2	0.0384	[-1.5694 -18.4996]	[0.2776 0.2627 0.2627 0.9198]	
3	0.3344	[-0.0148 -15.3005]	[0.1303 0.2647 0.2647 0.9584]	
4	0.4111	[-0.2817 -14.5136]	[0.0662 0.0536 0.0536 0.4303]	
5	0.1129	[-0.7303 -13.5903]	[0.1145 0.0096 0.0096 0.5683]	
6	0.0244	[0.3350 -12.2949]	[0.1864 0.4824 0.4824 2.1642]	

Table 1. Estimated component parameters where $\alpha_0 = 10^{-5}$. The first column represents the ID of components that are illustrated in Figure 2. π , μ and Σ indicate weight, location and shape of components, respectively.

gin of this division. The 2nd Voronoi region is very large and extends beyond the pulsar death line. The 3rd region contains most of the RRATs, XDINs, low-B magnetars and those RPPs close to the death line. There is again a 4th region populated by RPPs with a narrow \dot{P} range. About 10% of RRATs and GRPs overflow to this region. The 5th region mostly contains GRPs. The 6th region is predominantly occupied by AXPs/SGRs excluding the low-B magnetars.

3 RESULTS

In Figure 2, the pulsar families, components and Voronoi regions obtained from DPGMM are illustrated together with lines representing characteristic ages, magnetic field strengths and the death line. As we have discussed we have introduced 7 families of pulsars namely rotationally powered pulsars (RPPs) that involve millisecond pulsars, rotating radio transients (RRATs) and gamma-ray pulsars (GRPs) as well as conventional radio pulsars, and magnetars (AXPs, SGRs), X-ray dim INS (XDINs) and central compact objects (CCOs). As seen in Figure 2, DPGMM identifies 6 components for the value of the concentration parameter $\alpha_0 = 10^{-5}$. In this section we analyse whether these 6 components are linked to any parameters of pulsars other than P and \dot{P} (such as e.g. space velocity or surface temperature) that could attribute further meaning to the different components.

3.1 Pulsar distribution over the components

The distribution of all pulsars over the components obtained by DPGMM is given in Table 2. Accordingly, most of the ‘non-recycled’ RPPs detected in the radio band are located in the 3rd, 4th and 5th components. The ‘non-recycled’ GRPs are in the 5th component while the recycled ones are in the 1st component. RRATs populate mostly the 3rd component which they share with ‘low-B’ magnetars (J1647-4552, J0418+5732, J2301+5852 and J1822-1604), XDINs

and CCOs. ‘High-B’ AXPs and SGRs populate the 6th component. Moreover, most of the pulsars are grouped in the 3rd and 4th components that are located at the center of the diagram. There are fewer pulsars in other components relatively.

3.2 Effect of binary companion for recycled pulsars

The distribution of binary pulsars over components is given in Table 3. Accordingly, the binary pulsars are heavily grouped in the 1st and 2nd components where millisecond pulsars ‘live’. This, of course, is understood through the “recycling scenario” (Alpar et al. 1982) that address the very existence of these objects by spin-up of the neutron star through long-term accretion of matter and angular momentum from a binary companion. It is interesting, however, that both GMM and DPGMM found the millisecond pulsars are distributed into two components. What could be the underlying astrophysical distinction between these two components?

Almost all millisecond GRPs are located in the 1st component as seen in Table 3 and in Figure 2. This is obviously due to the higher rotational power, $L_{\text{sd}} = 4\pi^2 I\dot{P}/P^3$, of this component as well as the magnetic field strength at the light cylinder radius $R_{\text{LC}} = cP/2\pi$ given by

$$B_{\text{LC}} = \sqrt{\frac{24\pi^4 I\dot{P}}{c^3 P^5}}. \quad (24)$$

This can more readily be inferred from Figure 3. As $\{L_{\text{sd}}, B_{\text{LC}}\}$ are the linear functions of $\{P, \dot{P}\}$ in logarithmic scale

$$\begin{aligned} \log(B_{\text{LC}}) &\equiv \frac{1}{2} \log(\dot{P}) - \frac{5}{2} \log(P) \\ \log(L_{\text{sd}}) &\equiv \log(\dot{P}) - 3 \log(P) \end{aligned}$$

then $\mathbf{Y} = [\log(B_{\text{LC}}) \quad \log(L_{\text{sd}})]$ has also distribution of mixture of Gaussians. This is true for any data matrix \mathbf{Y} which is linearly related with \mathbf{X} . Therefore, an analysis in the $L_{\text{sd}} - B_{\text{LC}}$ parameter space are equivalent to the analysis in the $P - \dot{P}$ diagram. DPGMM is applied to the $L_{\text{sd}} - B_{\text{LC}}$ parameter space with $\alpha_0 = 10^{-5}$ and Voronoi regions of explored components are illustrated. The obtained classifications in $L_{\text{sd}} - B_{\text{LC}}$ parameter space are almost same as the classification in $P - \dot{P}$ parameter space as should be. As seen in the Figure 3, γ -ray emission can not be the underlying astrophysical cause for the existence of two separate components for millisecond pulsars; it will rather be a consequence.

The companion types of some binary pulsars have been detected and the distribution of those companions over the components is illustrated in Table 4. It is seen that there is a remarkable distinction between the properties of the companion objects in the two groups indicating to different astrophysical origins and recycling history. The 1st component is populated by millisecond pulsars with main sequence (MS), helium white dwarf (HE), carbon-oxygen white dwarf (CO) and ultra-light (UL) companions while lacking any neutron star companions. The 2nd component is populated by those with neutron star (NS) and white dwarf companions (CO and He), while having only 4 UL and no MS com-

Id	Normal	RRATs	GRPs	AXPs	SGRs	XDINs	CCOs	Comp. Total
1	137	0	38	0	0	0	0	175
2	73	0	2	0	0	0	0	75
3	703	21	0	4	0	6	3	737
4	906	12	15	0	0	0	0	933
5	142	1	62	0	0	0	0	205
6	21	1	0	10	8	1	0	41
Total	1982	35	117	14	8	7	3	2166

Table 2. The distribution of pulsar types over components. Columns represent pulsar types and rows represent components. Component IDs are placed at the first column. The number of pulsars that belong to each component is given at the last column. The number of pulsars that belong to a specific type is given in the last row.

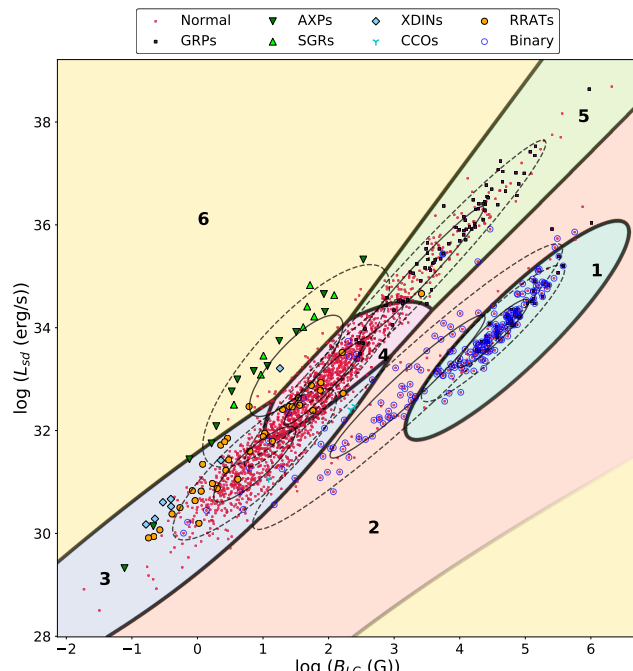


Figure 3. The magnetic field strength at the light cylinder radius vs the rotational power distribution of pulsars.

Id	Normal	GRPs	Comp. Total
1	103	32	135
2	51	0	51
3	13	0	13
4	6	0	6
5	3	1	4
6	0	0	0
Total	176	33	209

Table 3. The distribution of binary pulsar types over components. Component IDs are placed at the first column. The type of binary pulsars are located at the 2nd and the 3rd columns. The number of binary pulsars belonging to corresponding component is placed at the last column. The number of binary pulsars with a specific type is given in the last row.

panions. Lee et al. (2012) attributes the identification of two separate clusters to the chemical composition of the companions. This implies that millisecond pulsars in the 2nd component systematically had larger mass companions that lived shorter. Their larger periods (hence the smaller rotational

Id	MS	NS	CO	HE	UL
1	9	0	15	77	23
2	0	14	17	12	4
3	0	2	3	4	2
4	4	1	1	0	0
5	2	1	0	1	0
6	0	0	0	0	0
Total	15	18	36	94	29

Table 4. The distribution of companion types of binary pulsars over components. Component IDs are placed at the first column. Other columns indicate companion types: main-sequence (MS), neutron star (NS), carbon-oxygen (or ONeMg) white dwarf (CO), helium white dwarf (HE), and ultra-light companion or planet (UL). Companion types are obtained from Australia Telescope National Facility (ATNF) Pulsar Catalog (<http://www.atnf.csiro.au/research/pulsar/psrcat/>). The number of binary pulsars with a specific companion type is placed at the last row.

power and lack of gamma-emission) can be attributed to the shorter recycling history they suffered. It is remarkable that DPGMM distinguishes these two groups only through their spin parameter distributions.

3.3 Characteristic age and magnetic field

We calculated the mean values of characteristic age, $\tau_c \equiv P/2\dot{P}$, and magnetic dipole field strength as inferred under the assumption of a orthogonal rotating magnetic dipole model

$$B_d = \left(\frac{3c^3 I}{8\pi^2 R^6} \right)^{1/2} \sqrt{P\dot{P}} \quad (25)$$

of each component as shown in Table 1 where we assumed $I = 10^{45} \text{ g cm}^2$ and $R = 10^6 \text{ cm}$ for the moment of inertia and the radius of neutron stars, respectively. According to the table the age of a component with a larger ID number is smaller such that the oldest pulsars are in the 1st component while the youngest ones are in the 6th component. The table is arranged such that the magnetic dipole field strength of pulsars increase with their ID number so that youngest pulsars have largest field strengths. It is seen that the millisecond pulsars in the 2nd component have an order of magnitude larger magnetic dipole field strengths compared to those in the 1st component. According to our discussion in the previous subsection stronger fields can be un-

ID	Characteristic Age (yr)	Surface Magnetic Flux (Gauss)
1	4.49×10^9	2.52×10^8
2	1.35×10^9	2.96×10^9
3	3.06×10^7	7.04×10^{11}
4	2.70×10^6	1.28×10^{12}
5	1.15×10^5	2.21×10^{12}
6	6.76×10^4	3.35×10^{13}

Table 5. The average values of the characteristic age (year) and dipole magnetic field strength (Gauss) of components according to the mean values listed in Table 1 for each component.

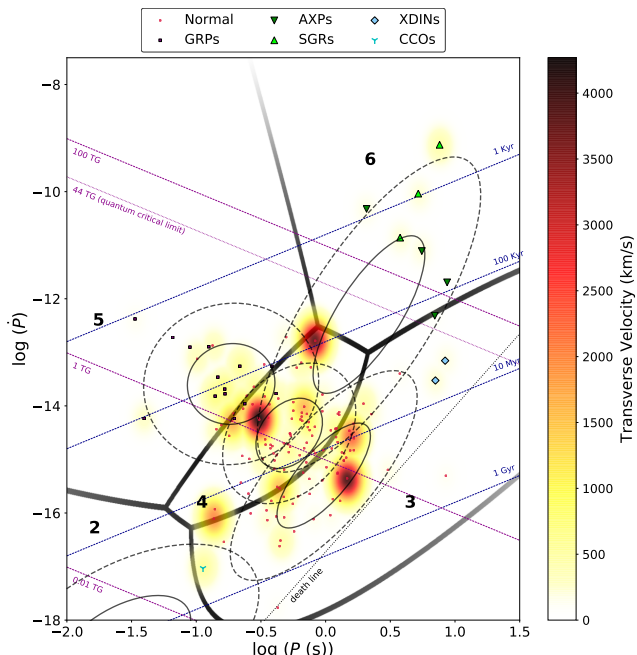


Figure 4. The transverse velocity of pulsars on the $P - \dot{P}$ diagram of non-recycled pulsars (the 3rd, 4th, 5th and 6th components). The color on the ‘heat map’ corresponds to the magnitude of the transverse velocity.

derstood as a consequence of the shorter ‘recycling’ episode these systems passed through.

3.4 Transverse velocity

According to the field burial model (Muslimov & Page 1995; Young & Chanmugam 1995; Geppert et al. 1999; Ho 2011) an initial, brief but intense, fallback accretion episode (Chevalier 1989) following the supernova explosion is important in shaping the magnetic fields of nascent pulsars. The amount of matter accreted determines how much the initial magnetic field is buried under the crust and thus the time-scale of diffusion of the field to the surface. Space velocities of pulsars due to the kick they receive during their birth may thus determine how much mass the neutron star can accrete, as the accretion rate is inversely proportional to the cube of the velocity in Bondi-Hoyle accretion. The field diffusion time-scale as inferred from the measured braking indices of young pulsars and the space velocities are inversely correlated (Güneydaş & Ekşioğlu 2013; Ekşioğlu 2017) as expected

Transverse Velocity (km/s)					
ID	N	μ_w	σ_w	μ	σ
3	50	363.3	677.4	335.5	625.4
4	71	373.6	570.1	470.0	753.6
5	20	359.1	265.4	302.6	248.8
6	6	231.5	79.7	252.2	141.0

Table 6. Statistics of transverse velocity (km/s) of non-recycled pulsars (the 3rd, 4th, 5th and 6th components). Here N stands for the number of pulsars with the measured speed in each component. μ , μ_w , σ and σ_w stand for mean, weighted mean, standard deviation and weighted standard deviation of the transverse speed, respectively. Weighted statistics are computed by weighting instances according to their probabilities of being in the corresponding component instead of Euclidean distance to the center of the component. The distribution of the transverse velocity is illustrated in Figure 4.

from the field-burial scenario. The question then naturally arises whether the space velocity of pulsars have any role in the observed diversity of pulsars.

In order to check this possibility we show the average transverse velocity of non-recycled pulsars (i.e. those in the 3rd, 4th, 5th and 6th components in the $P - \dot{P}$ diagram) as seen in Figure 4. The figure is colorized depending on the magnitude of transverse velocity of the corresponding pulsar so that color changes sequentially from yellow to red together with the magnitude. In addition, statistics of the transverse velocities for those components are also listed in Table 6. The weighted standard error is very large due to the low number of space velocity measurements in each group and the results may not be statistically significant. We see, however, that the space velocities of pulsars in the 4th component is the largest. We also see that the average speeds of pulsars in the 6th component is about half of those in the 4th component. The velocity data set is obtained from the same sources as mentioned in § 2.4.1.

3.5 Blackbody temperature

In Figure 5, the blackbody temperature of isolated pulsars belonging to the 3rd, 4th, 5th and 6th components are illustrated. Statistics of black body temperature of those components are also shown in Figure 5. As seen from the figure, most of the pulsars with measured black body temperatures are located in the 6th component and they are the hottest pulsars. In other words, SXP/SGRs are the hottest pulsar type. The blackbody temperatures of these pulsars are acquired from the sources mentioned in § 2.4.1 and also from Gonzalez et al. (2007); Kaspi & McLaughlin (2004); Webb et al. (2004); Hu et al. (2017); Li et al. (2005); Chang et al. (2011); Caraveo et al. (2010); Marelli et al. (2011); Gver et al. (2012); Posselt et al. (2012).

4 DISCUSSION

We have investigated the pulsar population with an unsupervised machine learning algorithm, Dirichlet process Gaussian mixture model (DPGMM). We confirmed the earlier result obtained with Gaussian mixture model (GMM) by Lee et al. (2012) that the millisecond pulsar population has

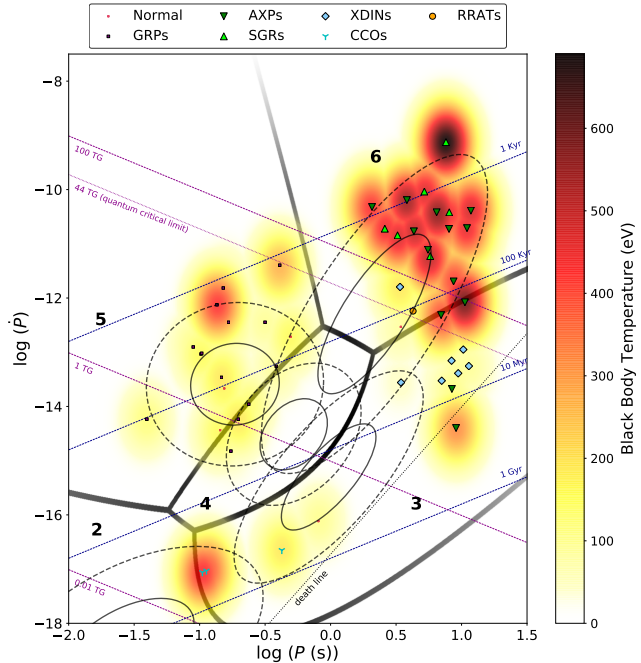


Figure 5. The blackbody temperature (eV) of non-recycled pulsars (the 3rd, 4th, 5th and 6th components). The color on the ‘heat map’ corresponds to the surface blackbody temperature of pulsars.

Blackbody temperature (eV)					
Id	<i>N</i>	μ_w	σ_w	μ	σ
3	14	138.2	83.7	219.2	175.0
4	3	126.3	55.4	128.7	67.7
5	14	157.5	51.0	172.0	84.4
6	19	334.1	171.3	395.5	166.5

Table 7. Statistics of blackbody temperature (eV) of non-recycled pulsars (the 3rd, 4th, 5th and 6th components). Here *N* stands for number of pulsars with the measured temperatures. μ , μ_w , σ and σ_w stand for mean, weighted mean, standard deviation and weighted standard deviation of temperature, respectively. Weighted statistics are computed by weighting instances according to their probabilities of being in the corresponding component instead of Euclidean distance to the center of the component. The distribution of blackbody temperature is illustrated in Figure 5.

two components and that the normal pulsar population consists of four components.

We have considered possible hidden parameters (space velocity and surface temperature) as possible underlying cause of the distinct components. We have found that the 4th component (see Figure 2) has about twice the average space velocity compared to the slowest component (the 6th) (see Figure 4) providing a marginal evidence that space velocities of young neutron stars could play a role in their astrophysical manifestations by controlling the total mass accreted during post-supernova fallback and the depth of field burial (Güneydaş & Ekşi 2013; Ekşi 2017). This indicates the pulsars in the 4th component suffered less superova fallback accretion and less field burial. Indeed the average magnetic field of pulsars in the 4th component are similar to those in the 5th component and are twice of those in the 3rd com-

ponent. If the magnetic fields of pulsars decay as they age within a timescale less than a million years, the difference in the magnetic fields of the 4th and 3rd components could be also attributed to the former systems being younger and subject to less field decay. Yet it is unlikely that the magnetic fields of typical pulsars decay in such short timescales favouring the idea that the space velocities could be the underlying reason for the difference in the magnetic fields of the 4th and 3rd components.

We note that the very high space velocities of CCOs imply that they are not likely to suffer very strong post-supernova fallback accretion. This does not neatly fit into the ‘field burial scenario’ (Muslimov & Page 1995; Geppert et al. 1999) as the small dipole fields of these objects, in this model, are attributed to very intense fallback accretion. This may indicate the role of the initial magnetic field and spin period as other parameters controlling the amount of the accreted fallback mass: The low magnetic fields and relatively slow initial periods of CCOs could allow them to accrete large amount of mass to bury their fields in spite of their large space velocities. Another solution high-speed-low-field puzzle could be that their dipole fields are in fact very strong but their rotation and spin axis are aligned to a very high precision such that the component of their dipole moment perpendicular to the rotation axis inferred from spin-down is so small. This idea, however, would work only in the vacuum dipole model i.e. if a corotating plasma does not exist around CCOs; MHD dipole model (Spitkovsky 2006) require non-vanishing spin-down even in the aligned case. This idea is worth considering given that only three of the CCOs show pulsations while there is evidence for strong magnetic fields (Shakura et al. 2012).

It is remarkable that the speed of objects in the 6th group is ‘typical’. This group involves AXP/SGRs which according to the magnetar model should have large space velocities, ~ 1000 km/s due to the “rocket effect” (Duncan & Thompson 1992; Thompson & Duncan 1993). This may be because it is their super-strong quadrupole fields, rather than the dipole fields, that distinguishes these objects from the rest of the isolated pulsars. The higher spin-down rates of these objects could then be attributed to additional torques, contributing to the magnetic dipole torque, due to winds (Harding et al. 1999; Thompson et al. 2000) or supernova fallback discs (Wang et al. 2006; Ertan et al. 2007).

The surface temperatures of pulsars in the 6th component are found to be relatively large (see Figure 5). This is an expected result as this component involves AXP/SGRs which, according to the magnetar model, have decaying fields. This also is expected according to the fallback disc model as a result of accretion (Alpar 2001; Chatterjee et al. 2000). A critical discrimination between the two models would be to compare the surface temperatures of HBPSR’s which presumably are not accreting objects, with those of AXP/SGRs. The upper limits on the temperatures of high magnetic field pulsars PSR B0154+61 (Gonzalez et al. 2004), J1814-1744 and J1847-0130 (Keane et al. 2013) imply that they are not significantly hotter than pulsars with lower magnetic fields thus raising the question why the fields of these objects do not decay and contribute to the X-ray luminosity. Yet the temperature of B1509-58 (Hu et al. 2017) lies between the temperatures of AXP/SGRs and typical RPPs, and the temperature of PSR J1119-6127 (Gonzalez

et al. 2005) is among the highest measured from typical RPPs. The observed pulsed fraction of this source is also higher than those of typical RPPs (Gonzalez et al. 2005) possibly indicating the role of strong fields and unlikely to be related to the presence of a putative fallback disc. Also, the recent analysis (Çerri-Serim et al. 2019) shows that the noise strength and X-ray luminosity magnetars lacks the correlation known to exist in accreting X-ray pulsars thus suggesting that they are not accreting.

If Voronoi regions do indeed have anything to do with the evolutionary connections among pulsar families, the 5th and the 6th regions may be considered as two different origins for young neutron stars on the $P - \dot{P}$ -diagram. A nascent neutron star may be born as a Crab-like GRP ($P_0 \sim 10$ ms, $\dot{P}_0 \sim 10^{-12}$ s/s) or as a magnetar ($P_0 \sim 0.5$ s, $\dot{P}_0 \sim 10^{-8}$ s/s assuming the field is not produced by the initial dynamo effect, but flux conservation (Ferrario & Wickramasinghe 2006) depending on its spin parameters, respectively. The classification presented here clearly relates low-B magnetars with XDINS and RRATs and implies they could descend from magnetars by field decay. Yet statistics suggests magnetars are much less common objects compared to XDINS and RRATs. This evolutionary scenario could, however, be validated only if magnetar stage is very short or there are many undiscovered transient magnetars. The recent identification of the high energy component in XDINS (Yoneyama et al. 2019) indeed suggests that magnetars and XDINS are evolutionarily linked.

There are, of course, strong selection effects on the representation of pulsars on the $P - \dot{P}$ diagram. CCO's, RRATs and XDINS should be much more common in the galaxy than they are detected. Yet it is not possible to do the similar analysis with a 'flux limited sample' at present as such filtering of data would result with much less instances of data than the model we employed, DPGMM, requires. Given that many types of pulsars are lower-represented in our sample, it may be argued that some of the components discovered by DPGMM are artefacts of describing an intrinsically non-Gaussian distribution. Yet, DPGMM classification we present here broadly coincides with the existing astrophysical classification despite it is an unsupervised model.

In summary, we have shown that an unsupervised machine learning algorithm, DPGMM, identifies 6 pulsar categories: two for recycled millisecond pulsars with different accretion histories; one roughly coincides with for XDINS, low-B magnetars and RRATs, but involves many RPPs as well; one involving the bulk of RPPs and a small fraction of RRATs; one involving the very young Crab-like RPPs including the bulk of the GRPs; and finally one that involve the AXPs/SGRs and HBPSRs.

ACKNOWLEDGEMENTS

KYE acknowledges support from TUBITAK, the national foundation of science in Turkey, with the project number 118F028. We thank M. Ali Alpar and Erbil Gürgencioğlu for useful discussion.

REFERENCES

Abdo A. A., Ackermann M., Ajello M., Allafort A., Baldini L., et al., 2010, *ApJ*, 725, L73

Abdo A. A., Ackermann M., Ajello M., Atwood W. B., Axelsson M., Baldini L., Ballet J., Barbiellini G., Baring M. G., Bastieri D., Baughman B. M., 2009, *Science*, 325, 848

Abdo A. A., Ackermann M., Ajello M., Atwood W. B., Axelsson M., Baldini L., Ballet J., Barbiellini G., Baring M. G., Bastieri D., et al. 2010, *ApJS*, 187, 460

Abdo A. A., Ajello M., Allafort A., Baldini L., Ballet J., Barbiellini G., Baring M. G., Bastieri D., Belfiore A., Belazzini R., et al. 2013, *ApJS*, 208, 17

Akaike H., 1974, *IEEE Transactions on Automatic Control*, 19, 716

Alpar M. A., 2001, *ApJ*, 554, 1245

Alpar M. A., Cheng A. F., Ruderman M. A., Shaham J., 1982, *Nature*, 300, 728

Alpar M. A., Ertan Ü., Çalışkan Ş., 2011, *ApJ*, 732, L4

Archibald R. F., Kaspi V. M., Tendulkar S. P., Scholz P., 2016, *ApJ*, 829, L21

Atwood W. B., Abdo A. A., Ackermann M., Althouse W., Anderson B., Axelsson M., Baldini L., Ballet J., Band D. L., Barbiellini G., 2009, *ApJ*, 697, 1071

Backer D. C., Kulkarni S. R., Heiles C., Davis M. M., Goss W. M., 1982, *Nature*, 300, 615

Bernal C. G., Page D., Lee W. H., 2012, *ArXiv e-prints*

Bhattacharya D., van den Heuvel E. P. J., 1991, *Physics Reports*, 203, 1

Bishop C., 2006, *Pattern Recognition and Machine Learning*. Springer

Blei D. M., Jordan M. I., 2006, *Bayesian Anal.*, 1, 121

Borghese A., Rea N., Coti Zelati F., Tiengo A., Turolla R., 2015, *ApJ*, 807, L20

Borghese A., Rea N., Coti Zelati F., Tiengo A., Turolla R., Zane S., 2017, *MNRAS*, 468, 2975

Borkowski K. J., Reynolds S. P., 2017, *ApJ*, 846, 13

Çerri-Serim D., Serim M. M., Şahiner Ş., İnam S. Ç., Baykal A., 2019, *MNRAS*, 485, 2

Şaşmaz Muş S., Göğüş E., 2010, *ApJ*, 723, 100

Camilo F., Ransom S. M., Halpern J. P., Reynolds J., 2007, *ApJ*, 666, L93

Camilo F., Ransom S. M., Halpern J. P., Reynolds J., Helfand D. J., Zimmerman N., Sarkissian J., 2006, *Nature*, 442, 892

Caraveo P. A., Luca A. D., Marelli M., Bignami G. F., Ray P. S., Parkinson P. M. S., Kanbach G., 2010, *The Astrophysical Journal*, 725, L6

Chang C., Pavlov G. G., Kargaltsev O., Shibakov Y. A., 2011, *The Astrophysical Journal*, 744, 81

Chatterjee P., Hernquist L., Narayan R., 2000, *ApJ*, 534, 373

Cheng K. S., Zhang L., 2001, *ApJ*, 562, 918

Chevalier R. A., 1989, *ApJ*, 346, 847

de Luca A., 2008, in C. Bassa, Z. Wang, A. Cumming, & V. M. Kaspi ed., 40 Years of Pulsars: Millisecond Pulsars, Magnetars and More Vol. 983 of American Institute of Physics Conference Series, Central Compact Objects in Supernova Remnants. pp 311–319

De Luca A., 2017, in *Journal of Physics Conference Series* Vol. 932 of *Journal of Physics Conference Series*, Central

compact objects in supernova remnants. p. 012006

De Maesschalck R., Jouan-Rimbaud D., Massart D. L., 2000, Chemometrics and intelligent laboratory systems, 50, 1

Del Pozzo W., Berry C. P. L., Ghosh A., Haines T. S., Singer L., Vecchio A., 2018, Monthly Notices of the Royal Astronomical Society, 479, 601

Deller A. T., Camilo F., Reynolds J. E., Halpern J. P., 2012, ArXiv e-prints

Dempster A. P., Laird N. M., Rubin D. B., 1977, Journal of the royal statistical society. Series B (methodological), pp 1–38

Duncan R. C., Thompson C., 1992, ApJ, 392, L9

Ekşi K. Y., 2017, MNRAS, 469, 1974

Ekşi K. Y., Alpar M. A., 2003, ApJ, 599, 450

Ertan Ü., Alpar M. A., 2003, ApJ, 593, L93

Ertan Ü., Ekşi K. Y., Erkut M. H., Alpar M. A., 2009, ApJ, 702, 1309

Ertan Ü., Erkut M. H., Ekşi K. Y., Alpar M. A., 2007, ApJ, 657, 441

Ferguson T. S., 1973, The annals of statistics, pp 209–230

Ferrario L., Wickramasinghe D., 2006, MNRAS, 367, 1323

Gavril F. P., Gonzalez M. E., Gotthelf E. V., Kaspi V. M., Livingstone M. A., Woods P. M., 2008, Science, 319, 1802

Gavril F. P., Kaspi V. M., Woods P. M., 2002, Nature, 419, 142

Gelman A., Stern H. S., Carlin J. B., Dunson D. B., Vehtari A., Rubin D. B., 2013, Bayesian data analysis. Chapman and Hall/CRC

Geppert U., Page D., Zannias T., 1999, A&A, 345, 847

Gonzalez M. E., Kaspi V. M., Camilo F., Gaensler B. M., Pivovaroff M. J., 2005, ApJ, 630, 489

Gonzalez M. E., Kaspi V. M., Camilo F., Gaensler B. M., Pivovaroff M. J., 2007, ApSS, 308, 89

Gonzalez M. E., Kaspi V. M., Lyne A. G., Pivovaroff M. J., 2004, ApJ, 610, L37

Gotthelf E. V., Halpern J. P., 2007, ApJ, 664, L35

Gotthelf E. V., Halpern J. P., 2009, ApJ, 695, L35

Gotthelf E. V., Halpern J. P., Alford J., 2013, ArXiv e-prints

Göögüs E., Lin L., Kaneko Y., Kouveliotou C., Watts A. L., Chakraborty M., Alpar M. A., Huppenkothen D., Roberts O. J., Younes G., van der Horst A. J., 2016, ApJ, 829, L25

Gourgouliatos K. N., Esposito P., 2018, ArXiv e-prints

Güneydaş A., Ekşi K. Y., 2013, MNRAS, 430, L59

Gver T., G E., zel F., 2012, Monthly Notices of the Royal Astronomical Society, 424, 210

Haberl F., 2007, ApSS, 308, 181

Halpern J. P., Gotthelf E. V., 2010, ApJ, 709, 436

Halpern J. P., Gotthelf E. V., 2011, ApJ, 733, L28

Hambaryan V., Suleimanov V., Haberl F., Schwope A. D., Neuhäuser R., Hohle M., Werner K., 2017, A&A, 601, A108

Harding A. K., 2013, Frontiers of Physics, 8, 679

Harding A. K., Contopoulos I., Kazanas D., 1999, ApJ, 525, L125

Helfand D. J., Chatterjee S., Brisken W. F., Camilo F., Reynolds J., van Kerkwijk M. H., Halpern J. P., Ransom S. M., 2007, ApJ, 662, 1198

Heller K., 2008, PhD thesis, University of London

Hewish A., Bell S. J., Pilkington J. D. H., Scott P. F., Collins R. A., 1968, Nature, 217, 709

Ho W. C. G., 2011, MNRAS, 414, 2567

Hu C.-P., Ng C.-Y., Takata J., Shannon R. M., Johnston S., 2017, ApJ, 838, 156

Hunter J. D., 2007, Computing In Science & Engineering, 9, 90

Igoshev A. P., Elfritz J. G., Popov S. B., 2016, MNRAS, 462, 3689

Igoshev A. P., Popov S. B., 2013, MNRAS, 434, 2229

Jones E., Oliphant T., Peterson P., et al., 2001–, SciPy: Open source scientific tools for Python

Kaplan D. L., 2008, in Bassa C., Wang Z., Cumming A., Kaspi V. M., eds, 40 Years of Pulsars: Millisecond Pulsars, Magnetars and More Vol. 983 of American Institute of Physics Conference Series, Nearby, Thermally Emitting Neutron Stars. pp 331–339

Kaspi V. M., 2010, Proceedings of the National Academy of Science, 107, 7147

Kaspi V. M., Beloborodov A. M., 2017, ARA&A, 55, 261

Kaspi V. M., McLaughlin M. A., 2004, The Astrophysical Journal, 618, L41

Keane E. F., Ludovici D. A., Eatough R. P., Kramer M., Lyne A. G., McLaughlin M. A., Stappers B. W., 2010, MNRAS, 401, 1057

Keane E. F., McLaughlin M. A., Kramer M., Stappers B. W., Bassa C. G., Purver M. B., Weltevrede P., 2013, ApJ, 764, 180

Kouveliotou C., Dieters S., Strohmayer T., van Paradijs J., Fishman G. J., Meegan C. A., Hurley K., Kommers J., Smith I., Frail D., Murakami T., 1998, Nature, 393, 235

Lee K. J., Guillemot L., Yue Y. L., Kramer M., Champion D. J., 2012, MNRAS, 424, 2832

Levin L., Bailes M., Bates S., Bhat N. D. R., Burgay M., Burke-Spolaor S., D'Amico N., Johnston S., Keith M., Kramer M., Milia S., Possenti A., Rea N., Stappers B., van Straten W., 2010, ApJ, 721, L33

Li X. H., Lu F. J., Li T. P., 2005, The Astrophysical Journal, 628, 931

McKinney W., et al., 2010, in Proceedings of the 9th Python in Science Conference Vol. 445, Data structures for statistical computing in python. pp 51–56

Mahalanobis P. C., 1936 On the generalized distance in statistics

Manchester R. N., 2017, in Journal of Physics Conference Series Vol. 932 of Journal of Physics Conference Series, 50 Years of Pulsars!. p. 012001

Marelli M., Luca A. D., Caraveo P. A., 2011, The Astrophysical Journal, 733, 82

Martin J., Rea N., Torres D. F., Papitto A., 2014, MNRAS, 444, 2910

McLaughlin M. A., Lyne A. G., Lorimer D. R., Kramer M., Faulkner A. J., Manchester R. N., Cordes J. M., Camilo F., Possenti A., Stairs I. H., Hobbs G., D'Amico N., Burgay M., O'Brien J. T., 2006, Nature, 439, 817

McLaughlin M. A., Stairs I. H., Kaspi V. M., Lorimer D. R., Kramer M., Lyne A. G., Manchester R. N., Camilo F., Hobbs G., Possenti A., D'Amico N., Faulkner A. J., 2003, ApJ, 591, L135

Mereghetti S., 2008, A&ARv, 15, 225

Mereghetti S., 2011, Astrophysics and Space Science Proceedings, 21, 345

Mereghetti S., Pons J. A., Melatos A., 2015, Space Science Reviews, 191, 315

Muslimov A., Page D., 1995, *ApJ*, 440, L77

Neal R. M., 2000, *Journal of Computational and Graphical Statistics*, 9, 249

Ng C.-Y., Kaspi V. M., 2011, in E. Göğüş, T. Belloni, Uuml. Ertan ed., *American Institute of Physics Conference Series* Vol. 1379 of *American Institute of Physics Conference Series*, High Magnetic Field Rotation-powered Pulsars. pp 60–69

Olausen S. A., Kaspi V. M., 2014, *ApJS*, 212, 6

Oliphant T. E., 2006, *A guide to NumPy*. Vol. 1, Trelgol Publishing USA

Özel F., 2013, *Reports on Progress in Physics*, 76, 016901

Paczynski B., 1992, *Acta Astronomica*, 42, 145

Pedregosa F., Varoquaux G., Gramfort A., Michel V., Thirion B., Grisel O., Blondel M., Prettenhofer P., Weiss R., Dubourg V., Vanderplas J., Passos A., Cournapeau D., Brucher M., Perrot M., Duchesnay E., 2011, *Journal of Machine Learning Research*, 12, 2825

Pérez F., Granger B. E., 2007, *Computing in Science & Engineering*, 9

Pivovaroff M. J., Kaspi V. M., Camilo F., 2000, *ApJ*, 535, 379

Popov S. B., 2008, *Physics of Particles and Nuclei*, 39, 1136

Posselt B., Arumugasamy P., Pavlov G. G., Manchester R. N., Shannon R. M., Kargaltsev O., 2012, *The Astrophysical Journal*, 761, 117

Potekhin A. Y., De Luca A., Pons J. A., 2015, *Space Science Reviews*, 191, 171

Press W. H., Teukolsky S. A., Vetterling W. T., Flannery B. P., 2007, *Numerical recipes 3rd edition: The art of scientific computing*. Cambridge university press

Raiffa H., Schlaifer R., 1961, *Applied statistical decision theory*

Rasmussen C. E., 2000, in *Advances in neural information processing systems* The infinite gaussian mixture model. pp 554–560

Rea N., 2014, *Astronomische Nachrichten*, 335, 329

Rea N., Borghese A., Esposito P., Coti Zelati F., Bachetti M., Israel G. L., De Luca A., 2016, *ApJ*, 828, L13

Rea N., Esposito P., Turolla R., Israel G. L., Zane S., Stella L., Mereghetti S., Tiengo A., Götz D., Göğüş E., Kouveliotou C., 2010, *Science*, 330, 944

Rodríguez Castillo G. A., Israel G. L., Tiengo A., Salvetti D., Turolla R., Zane S., Rea N., Esposito P., Mereghetti S., Perna R., Stella L., Pons J. A., Campana S., Götz D., Motta S., 2016, *MNRAS*, 456, 4145

Safi-Harb S., 2017, in *Journal of Physics Conference Series* Vol. 932 of *Journal of Physics Conference Series*, Neutron stars: Observational diversity and evolution. p. 012005

Schwarz G., 1978, *Ann. Statist.*, 6, 461

Shabaltas N., Lai D., 2011, ArXiv e-prints

Shakura N., Postnov K., Kochetkova A., Hjalmarsdotter L., 2012, *MNRAS*, 420, 216

Spitkovsky A., 2006, *ApJ*, 648, L51

Tan C. M., Bassa C. G., Cooper S., Dijkema T. J., Esposito P., Hessels J. W. T., Kondratiev V. I., Kramer M., Michilli D., Sanidas S., Shimwell T. W., 2018, *ApJ*, 866, 54

Tauris T. M., van den Heuvel E. P. J., 2006, Formation and evolution of compact stellar X-ray sources. pp 623–665

Tendulkar S. P., Cameron P. B., Kulkarni S. R., 2012, *ApJ*, 761, 76

Tendulkar S. P., Cameron P. B., Kulkarni S. R., 2013, *ApJ*, 772, 31

Tetzlaff N., Eisenbeiss T., Neuhäuser R., Hohle M. M., 2011, *MNRAS*, 417, 617

Tetzlaff N., Neuhäuser R., Hohle M. M., Maciejewski G., 2010, *MNRAS*, 402, 2369

Tetzlaff N., Schmidt J. G., Hohle M. M., Neuhäuser R., 2012, *Publications of the Astronomical Society of Australia*, 29, 98

Thompson C., Duncan R. C., 1993, *ApJ*, 408, 194

Thompson C., Duncan R. C., 1995, *MNRAS*, 275, 255

Thompson C., Duncan R. C., 1996, *ApJ*, 473, 322

Thompson C., Duncan R. C., Woods P. M., Kouveliotou C., Finger M. H., van Paradijs J., 2000, *ApJ*, 543, 340

Tong H., Song L. M., Xu R. X., 2011, *ApJ*, 738, 31

Torres D. F., 2017, *ApJ*, 835, 54

Torres-Forné A., Cerdá-Durán P., Pons J. A., Font J. A., 2016, *MNRAS*, 456, 3813

Turolla R., 2009, in Becker W., ed., *Astrophysics and Space Science Library* Vol. 357 of *Astrophysics and Space Science Library*, Isolated Neutron Stars: The Challenge of Simplicity. p. 141

Turolla R., Esposito P., 2013, *International Journal of Modern Physics D*, 22, 1330024

Turolla R., Zane S., Watts A. L., 2015, *Reports on Progress in Physics*, 78, 116901

van der Walt S., Schönberger J. L., Nunez-Iglesias J., Boulogne F., Warner J. D., Yager N., Gouillart E., Yu T., the scikit-image contributors 2014, *PeerJ*, 2, e453

Viganò D., Pons J. A., 2012, *MNRAS*, 425, 2487

Viganò D., Rea N., Pons J. A., Perna R., Aguilera D. N., Miralles J. A., 2013, *MNRAS*, 434, 123

Vink J., Kuiper L., 2006, *MNRAS*, 370, L14

Wang Z., Chakrabarty D., Kaplan D. L., 2006, *Nature*, 440, 772

Waskom M., et al., 2017, *mwaskom/seaborn: v0.8.1* (September 2017)

Webb N. A., Olive J.-F., Barret D., 2004, *A&A*, 417, 181

Witten I. H., Frank E., Hall M. A., Pal C. J., 2016, *Data Mining: Practical machine learning tools and techniques*. Morgan Kaufmann

Woods P. M., Thompson C., 2006, *Soft gamma repeaters and anomalous X-ray pulsars: magnetar candidates*. Cambridge University Press, pp 547–586

Yoneyama T., Hayashida K., Nakajima H., Matsumoto H., 2019, *PASJ*, 71, 17

Young E. J., Channugam G., 1995, *ApJ*, 442, L53

Zhang L., Cheng K. S., 1997, *ApJ*, 487, 370